Available online at www.sciencedirect.com
SCIENCE DIRECT®
Journal of Power Sources 137 (2004) 9–16
JOURNAL OF POWER SOURCES
www.elsevier.com/locate/jpowsour

Studies on the initial behaviours of the molten carbonate fuel cell

Ye-Ro Lee [a], In-Goo Kim [a], Gui-Yung Chung [a,*], Choong-Gon Lee [b], Hee-Chun Lim [b], Tae-Hoon Lim [c], Suk-Woo Nam [c], Seong-Ahn Hong [c]

[a] *Department of Chemical Engineering, Hong-Ik University, 72-1 Sangsudong, Mapoku, Seoul, 121-791 South Korea*
[b] *Korea Electric Power Research Institute (KEPRI), 103-16 Munjidong, Yuseonggu, Daejeon, 305-380, South Korea*
[c] *Battery and Fuel Cell Research Center, Korea Institute of Science and Technology (KIST), P.O. Box 131 Cheongryang, Seoul, 130-650, South Korea*

Received 12 February 2004; accepted 19 May 2004
Available online 1 August 2004

Abstract

Mathematical modelling of the unsteady-state of a unit molten carbonate fuel cell (MCFC) has been made. The behaviour of the fuel cell at the beginning of the operation is observed. The effects of the molar flow rates of gases and the utilization of fuel gas are studied. The current density decreases with time and reaches a steady-state value of 0.14 A cm^{-2} at 0.58 s for the chosen reference conditions. As the inlet gas-flow rates or the hydrogen utilization are increased, the time required to reach a steady-state decreases. With increased flow rates of the anode and cathode gases, the average current density is high and the total concentration is low. The current density increases with increasing utilization of hydrogen.
© 2004 Elsevier B.V. All rights reserved.

Keywords: Molten carbonate fuel cell; Unsteady-state; Intial behaviour; Gas flow rate; Hydrogen utilization

1. Introduction

The molten carbonate fuel cell (MCFC) is considered to be a second-generation fuel cell. It has high efficiency and lower emissions of NO_x and SO_x. It also has applicability to both small- and large-scale plants [1]. At present, the technology of MCFCs is at the stage of scale up to commercialization. In this respect, the modelling of the system becomes important.

In modelling and estimating the performance of MCFCs, many operating parameters are related to each other. Parameters such as mass- and heat-transfer, chemical reactions and electrical correlations are used to estimate performances of MCFC. Many numerical analyses of MCFC have been undertaken. For example, Sampath and Sammels [2] have developed a numerical analysis model for an isothermal unit fuel cell, Watanabe et al. [3] have analyzed the cooling characteristics of the cathode, Wolf and Wilemski [4] have studied temperature distributions, and Cao and Masubuchi [5] have defined the dynamic characteristics of temperature in a unit cell.

Many cell and stack models are based on macroscopic balances of the electrochemical reactors. In other words, a simplified model of cell performance has been applied. On the other hand, Kobayashi et al. [6] and Fujimura et al. [7] have calculated temperature distributions of single cells and stacks by applying mass-transfer to the chemical reactions that occur in the fuel cell and have applied a thin-film cylindrical-pore model to study the relation between current density and cell voltage. Likewise, micromodels of the electrodekinetics [6–10] and the effects of the gas cross-over phenomena through the electrolyte have been examined [11]. In addition, Yoshiba et al. [3] have used numerical analysis to compare the stack performance of various gas-flow types.

In this research, mathematical modelling of a parallel-flow unsteady-state MCFC has been performed. The behaviour of the fuel cell in terms of changes in the electrochemical reactions with time, distribution of the current density and cell temperature and mole fractions of gases at the initial stage of the operation are observed. Such a study of the intial behaviour of the system will help understand how the

* Corresponding author. Tel.: +82 2 320 1681; fax: +82 2 320 1191.
E-mail address: gychung@hongik.ac.kr (G.-Y. Chung).

0378-7753/$ – see front matter © 2004 Elsevier B.V. All rights reserved.
doi:10.1016/j.jpowsour.2004.05.044

system will recover to the steady-state after sudden changes in operating conditions.

2. Mathematical modelling

2.1. MCFC system

The reactions in an MCFC are reduction of oxidant gas at the cathode (positive) electrode and oxidation of fuel gas at the anode (negative) electrode. The oxidant gas in the cathode gas channel forms carbonate ions, as shown by Eq. (1). These ions are transported to the anode through the electrolyte matrix, and water and carbon dioxide are formed in the anode reaction, as shown by Eq. (2), i.e.,

$$\text{Cathode}: \quad CO_2 + \tfrac{1}{2}O_2 + 2e^- \rightarrow {CO_3}^{2-} \tag{1}$$

$$\text{Anode}: \quad H_2 + {CO_3}^{2-} \rightarrow CO_2 + H_2O + 2e^- \tag{2}$$

The anode reactions also include the water–gas shift reaction, whereby the carbon dioxide formed via Eq. (2) reacts with hydrogen and produces carbon monoxide and water. This shift reaction provides the additional fuel, i.e., H_2 in the anode gas [12]. Because of this, the utilization of fuel in MCFC can exceed the utilization of H_2 based on the inlet concentration of H_2.

Heat is generated in the electrode–electrolyte plate by the electrochemical reaction and the water–gas shift reaction. The generated heat is transferred to the other parts of fuel cell by conduction, convection and radiation. Unsteady-state energy balance equations can be formulated to include these heat-transfer processes and time-change terms. Similar equations can also be developed for the convectional and the diffusional transfers, the electrochemical reaction and the time-change terms.

A schematic diagram of a parallel-flow unit MCFC with a cross-sectional area of 10 cm × 10 cm is shown in Fig. 1. Most assumptions used in this modelling are the same as those used in steady-state modelling [13–16]. Rectangular gas channels are assumed, and the anode, electrolyte plate and cathode are considered to be one uniform electrode–electrolyte plate. The conduction heat-transfer in this electrode–electrolyte plate is examined. The thermal conductivity of the electrode–electrolyte plate is calculated as a combination of the thermal conductivities of the anode, the electrolyte and the cathode. The properties of the anode gas, the electrode–electrolyte plate and the cathode gas are assumed to be constant along the thickness direction. Only convectional heat transter is considered in the gas channels. Heat loss from the side of fuel cell is ignored. The same parameter values used in our previous steady-state analyses [13–16] are used in this modelling. The dimensions and operating conditions of the modelling are given in Table 1.

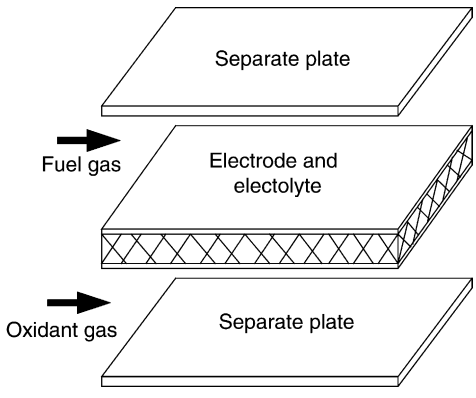

Fig. 1. Schematic diagram of co-flow type MCFC.

Table 1
Dimensions and conditions of MCFC used in mathematical modelling

Length (L, cm)		10
Width (W, cm)		10
Thickness (cm)	Separator (b_s)	0.2
	Gas channel (b_g)	0.2
	Anode electrode (b_{ea})	0.07
	Electrolyte plate (b_{em}): cathode electrode (b_{ec})	0.1: 0.06
Flow rate (mol h^{-1})	Anode gas	0.88
	Cathode gas	1.05
Composition	Anode gas	H_2 0.68; CO_2 0.08; CO 0.12; H_2O 0.12
	Cathode gas	O_2 0.33, CO_2 0.67

2.2. Governing equations

The equation of the mass and energy balances are established by adding time-change terms to the steady-state equations.

2.2.1. Mass-balance equations and the current density–voltage relationship

The mass-balance equation for the cathode gas includes the convection mass-transfer, the electrochemical reaction and the time-change term. The anode mass-balance equation includes a term for the water gas shift reaction.

For cathode gas:

$$-\frac{1}{\Delta y}\frac{\partial(n_c x_k)}{\partial x} + v_{Ec,k}\frac{i}{2F} = \frac{d(C_{ck})}{dt} \tag{3}$$

where: v_{Eck} is the stoichiometric coefficient of the k-component concentration in the anode gas; n_c is the molar flow rate (gmol/s cm^3), C_{ck} is the k-component concentration in the cathode gas (gmol/cm^3), F is the Faraday constant.

For anode gas:

The amount of mass change due to the water–gas shift reaction is added to the mass-balance equation of anode gas,

i.e.,

$$-\frac{1}{\Delta y}\frac{\partial(n_a x_k)}{\partial x}+\upsilon_{Ea,k}\frac{i}{2F}+\upsilon_{sk}\frac{n_s}{\Delta x\Delta y}=\frac{d(C_{ak})}{dt} \quad (4)$$

where: C_{ak} is the k-component concentration in the anode gas; υ_{sk} is the stoichiometric coefficient in the water–gas shift reaction. The molar flow rate of hydrogen in the anode gas ($n_a x_{H_2}$) at an arbitrary position is calculated using the total conversion of hydrogen at the exit of gas channel. The conversion of hydrogen (x_{H_2}) in each element (dx) of the gas channel is deduced for the number of elements (N: 20 in this research) and the total conversion of hydrogen (U_{H_2}) as given by:

$$x=1-(1-U_{H_2})^{1/N} \quad (5)$$

The molar flow rates of CO_2, CO, H_2O and O_2 in the cathode gas and CO_2 in the anode gas are calculated from a combination of the electrochemical reaction and the conversion of hydrogen. For the water–gas shift reaction, the equation of equilibrium-state is used [17,18].

The current density and the cell voltage have the following relationship:

$$V=(V_{cN}-V_{aN})-iZ \quad (6)$$

The equilibrium potentials of the anode and the cathode, V_{aN} and V_{cN}, are derived from the Nernst equation [12]. The effective cell resistance, Z in Eq. (6), is the sum of the ohmic resistance (R_{ohm}) and the polarization resistances (Z_a and Z_c). The latter, which has been suggested by Selman [19] to be a function of the partial pressures of each component and temperature, are used in this research, i.e.,

$$Z_a=2\times0.4567\times10^{-7}(p_{H_2})^{-1.801}\times(p_{CO})^{1.533}(p_{CO_2})^{-1.480}\exp\left(\frac{13140}{T}\right) \quad (7)$$

$$Z_c=7.504\times10^{-6}(p_{O_2})^{-0.43}(p_{CO_2})^{-0.09}\exp\left(\frac{9361}{T}\right) \quad (8)$$

Substituting V_{cN}, V_{aN}, R_{ohm} and Z into the Eq. (6), the following equation is obtained:

$$V=(V_a^o-V_c^o)+\frac{RT}{2F}\ln\left(\frac{X_{cC}X_O^{1/2}X_H}{X_W X_{aC}}\right)-iZ \quad (9)$$

Then, the local current density can be calculated with the cell voltage and the gas compositions.

2.2.2. Energy-balance equations

The equations of energy balance for the upper and the lower separators, anode and cathode gases and the electrode–electrolyte plate are developed. In the same way as the mass-balance equations, the energy-balance equations are built by adding time-change items to the steady-state equations [20,21].

For cathode gas:

$$-\frac{\partial}{\partial x}(m_c C_{pc}T_{gc})+h_{egc}(T_e-T_{gc})+h_{sgc}(T_s-T_{gc})+\sum_k G_c C_{pc,k}b_g T_{gc}+\frac{Q_s}{W\Delta y}=b_g\rho_{gc}C_{pgc}\frac{dT_{gc}}{dt} \quad (10)$$

b.c. at $x=0$, all y; $T_{gc}=T_i$

The heat of electrochemical reaction, q_E (J cm^{-2}), is obtained as follows [12].

$$q_E=i\left(-\frac{\Delta H_E}{2F}+V\right) \quad (11)$$

where, ΔH_E (J/mol) is the enthalpy change caused by the electrochemical reaction [17].

For anode gas:

The energy balance equation for the anode gas includes the heat of the shift reaction as the mass-balance equation.

$$-\frac{\partial}{\partial x}(m_a C_{pa}T_{ga})+h_{ega}(T_e-T_{ga})+h_{sga}(T_s-T_{ga})+\sum_k G_a C_{pa,k}b_g T_{ga}+\frac{Q_s}{W\Delta x}=b_g\rho_{ga}C_{pga}\frac{dT_{ga}}{dt} \quad (12)$$

Boundary conditions: at $x=0$, all y; $T_{ga}=T_i$.

For the upper and the lower separators:

$$-\frac{\partial^2 T_s}{\partial x^2}+\frac{\partial^2 T_s}{\partial y^2}+\frac{h_{res}}{b_s k_s}(T_e-T_s)+\frac{h_{rsg}}{b_s k_s}(T_g-T_s)+\frac{h_{rsb}}{b_s k_s}(T_b-T_s)=\rho_s C_{ps}\frac{dT_s}{dt} \quad (13)$$

Boundary condition: at $x=0$ and $x=L$, all y; $\partial T_s/\partial x=0$; at all x, $y=0$ and $y=W$; $\partial T_s/\partial y=0$.

For the electrode–electrolyte plate:

$$-\frac{\partial^2 T_e}{\partial x^2}+\frac{\partial^2 T_e}{\partial y^2}+\frac{h_{res}}{b_e k_e}(T_e-T_s)+\frac{h_{res}}{b_e k_e}(T_e-T_s)+\frac{h_{res}}{b_e k_e}(T_e-T_{ga})+\frac{h_{ega}}{b_e k_e}(T_e-T_{ga})+\frac{h_{egc}}{b_e k_e}(T_e-T_{gc})+\frac{q_E}{b_e k_e}=\rho_e C_{pe}\frac{dT_e}{dt} \quad (14)$$

at $x=0$ and $x=L$, all y; $\partial T_e/\partial x=0$;
at x, $y=0$ and $y=W$; $y=W$; all y; $\partial T_e/\partial y=0$.

2.3. Analytical methods of calculations

All mass- and energy-balance equations are changed into dimensionless equations and then into finite difference equations. The current density, temperature, power and conversion of gases are obtained as a function of time. The time required to reach a steady-state is also obtained. The calculations are performed with a fixed value for the cell voltage [13–16].

The initial concentrations of the gases are obtained with the equation of state, and all the initial temperatures in the

interiors and the boundaries of the MCFC are assumed to be 923 K (650 °C).

The degree of freedom in the system is one. Equations for a unit MCFC are solved after fixing one parameter, i.e., the cell voltage. The current density at time $(t+\Delta t)$ is obtained using Eq. (9). For calculations of the time changes of the concentrations of the anode and cathode gases, the molar flow rates of gases are estimated using the utilization of hydrogen as in Eq. (5). The reference total utilization of hydrogen is assumed to have an experimental value of 0.4. In case of the anode gas conversion by the water–gas shift reaction is calculated using the equilibrium-state equation. Then, the concentration and compositions of the anode gas can be calculated. Similar calculations are undertaken for the cathode gas. Using the obtained values, current density distributions are calculated by a trial-and-error method.

Temperature distributions can be calculated by means of Eqs. (10)–(14) All these calculation steps are repeated for increasing time. When the changes in the molar flow rates of both gases become negligible, the calculations are stopped and it is assumed that a steady-state is reached. Dimensions, flow rates and gas compositions of the unit MCFC used in the modelling are in Table 1.

3. Results and discussion

Equations for the 10 cm × 10 cm MCFC unit cell were solved after fixing one parameter, i.e., the cell voltage, 0.93 V. Cell performances, the time reaching a steady-state, gas compositions and conversions were calculated and compared at different utilizations of hydrogen and molar flow rates of the fuel gas.

3.1. Time changes of current density and gas compositions

Distributions of hydrogen composition along the direction of gas flow at different times are given in Fig. 2. Calculations were made at a constant cell voltage of 0.93 V. The time to reach a steady-state was taken as the time when the changes in gas compositions in the gas channel became negligible with respect to time. The graph shows that the time changes of the gas composition along the direction of gas flow become small as the system approaches a steady-state. Here, 5.8 s is the time to reach a steady-state when the molar flow rate of the cathode gas is 0.44 mol h^{-1} and the fuel gas utilization is 0.4. It reaches a steady-state very quickly because the size of fuel cell is small and the flow rate of fuel gas is large. At the initial stages of operation, the slope of the distribution curve is small, but increases slightly as time passes.

The distribution of current density along the direction of gas flow at different times is presented in Fig. 3. The trend is similar as that in Fig. 2. This is because the current density is related to the amount of reacted hydrogen in the anode. As the anode gas flows, it is consumed by the electrochemical reaction in the electrode–electrolyte plate. Thus, the amount of hydrogen decreases and the current density becomes low along the direction of gas flow.

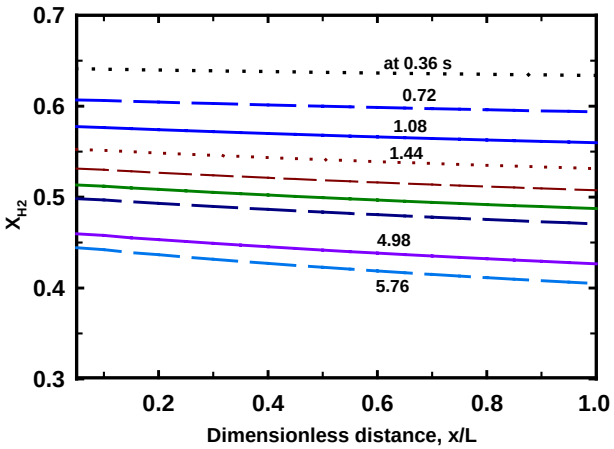

Fig. 2. Distribution of mole fraction of hydrogen (x_{H_2}) in anode gas along direction of gas flow at different times. Anode gas-flow rate = 0.44 mol h^{-1} (i.e., $0.5n_{a,o}$); cell voltage = 0.93 V, U_{H_2} = 0.4.

3.2. Effects of gas velocity

As the velocities of the anode and the cathode gases become fast, the time to reach a steady-state become short. The effects of the inlet molar flow rates of anode gas on the gas fractions along the direction of gas flow after reaching a steady-state are shown in Fig. 4. Here, $n_{a,o}$ refers to the reference molar flow rate of anode gas, i.e., 0.88 mol h^{-1} The cathode gas-flow rate, $n_{c,o}$ is fixed. The sum of the fractions of gases, such as H_2, CO, CO_2 and H_2O in Fig. 4(a)–(d) should be almost one.

When the anode flow rate is high, the fraction of hydrogen is large and the difference from the inlet fraction of 0.68 becomes small. Hence, the curve at $n_{a,o}$ is above the curves at $0.5n_{a,o}$ and $0.1n_{a,o}$. Even though the slopes of curves

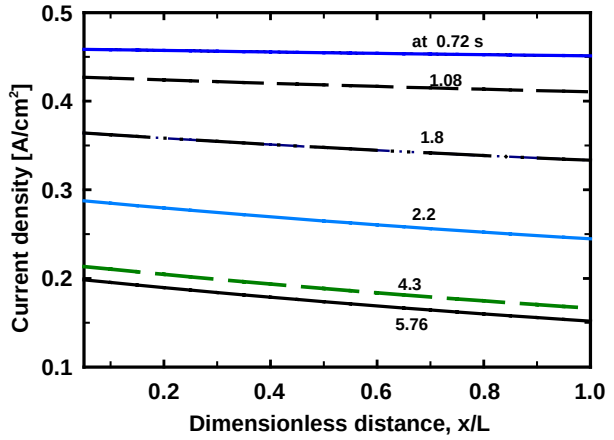

Fig. 3. Distribution of current density along direction of gas flow at different times.

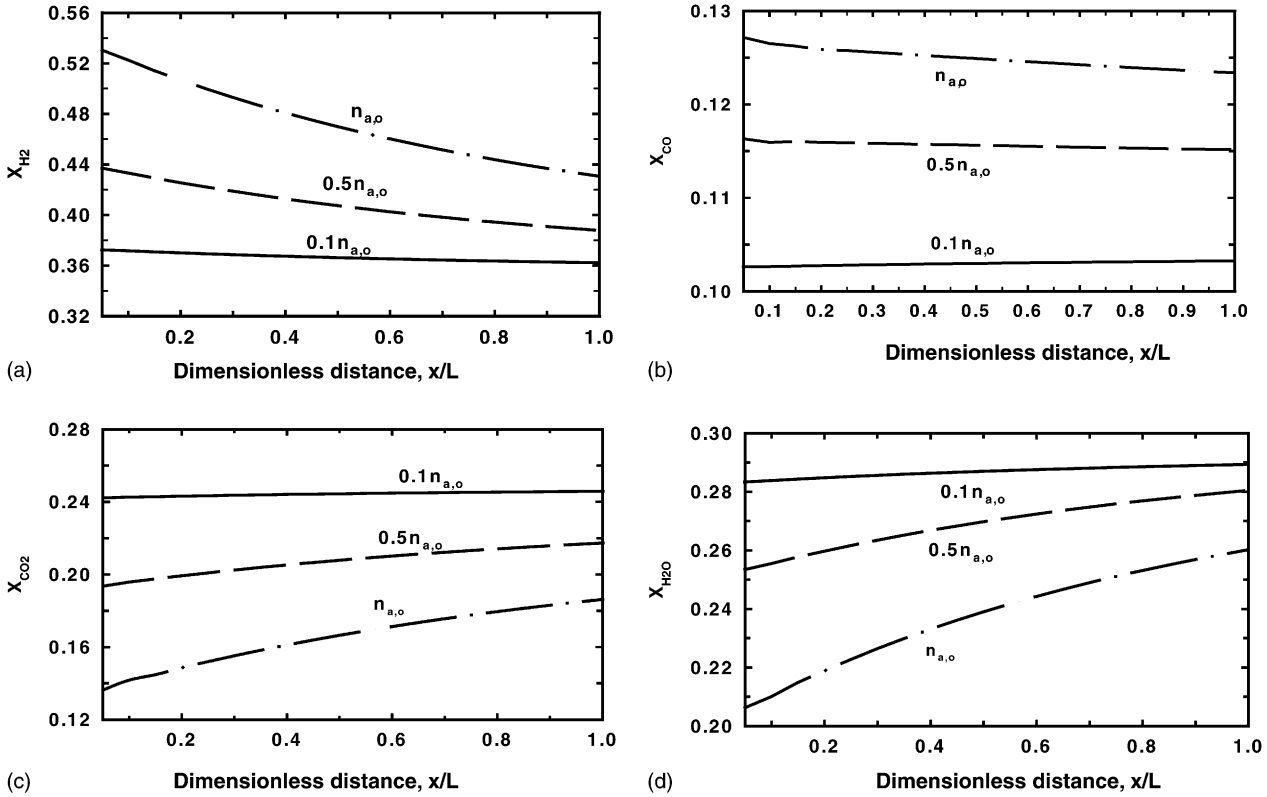

Fig. 4. Steady-state distribution of mole fraction of each component in anode gas along direction of gas flow at $n_{a,o}$, $0.5n_{a,o}$ and $0.1n_{a,o}$. (a) H_2; (b) CO; (c) CO_2; and (d) H_2O. Here, $n_{a,o}$ is the reference inlet anode gas-flow rate, i.e., 0.88 mol h^{-1}. Flow rates of anode and cathode gases are changed in the same ratio.

are rather uniform, they are slightly larger at the entrance. This is due to the high concentration of hydrogen at the entrance and it is related to the high current density at the entrance. Additionally, when the anode flow rate is high, the rate of hydrogen consumption is faster and the distribution curve changes more rapidly along the *x*-direction as shown in Fig. 4a. CO in the anode is related to the water gas shift reaction in the anode gas. Even though the changes in the slopes of the curves in Fig. 4b are very small, the trends are similar to those of hydrogen in Fig. 4a.

As mentioned above, the fraction of hydrogen at the entrance is large when the anode gas-flow rate is high. By contrast, the amount of carbonate ions from the cathode is relatively constant, since the cathode gas-flow rate has been fixed. Hence, when the anode flow rate is large, the fractions of CO_2 and H_2O in the anode gas, which are generated from the carbonate ions, are small as shown in Fig. 4(c) and (d).

As mentioned above, the molar flow rate at the entrance will affect the time taken to reach a steady-state and the concentration distribution in the gas channel. The change in the total anode concentration with time at the centre ($x = 0.5\,L$) of the cell for different molar flow rates of anode gas is given in Fig. 5. The molar flow rate of the cathode gas changes in the same ratio as that of the anode gas. As time passes, the total anode concentration increases and reaches a steady-state. On the other hand, the total cathode concentration decreases and reaches a steady-state value. This is because the total mole number of anode gas increases and the total mole number of cathode gas decreases after the electrochemical reaction. As shown in Fig. 4, when the molar flow rate is large, the time to reach a steady-state is short. In spite of the large molar flow rate, the concentration is lower

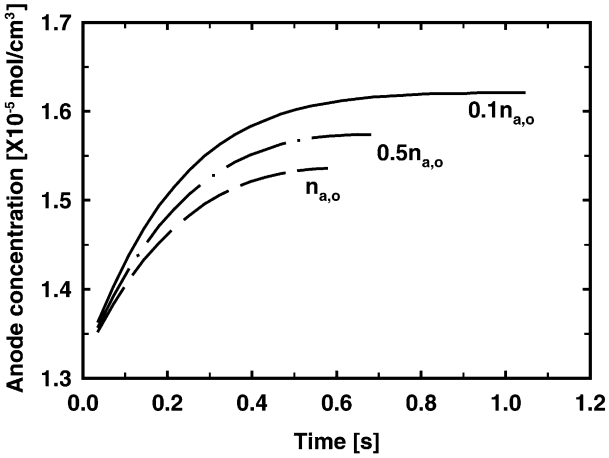

Fig. 5. Time changes of anode concentration at centre ($x/L = 0.5$) of cell at $n_{a,o}$, $0.5n_{a,o}$ and $0.1n_{a,o}$. Here, $n_{a,o}$ is reference inlet anode gas-flow rate, i.e., 0.88 mol h^{-1}. Flow rates of anode and cathode gases are changed in the same ratio.

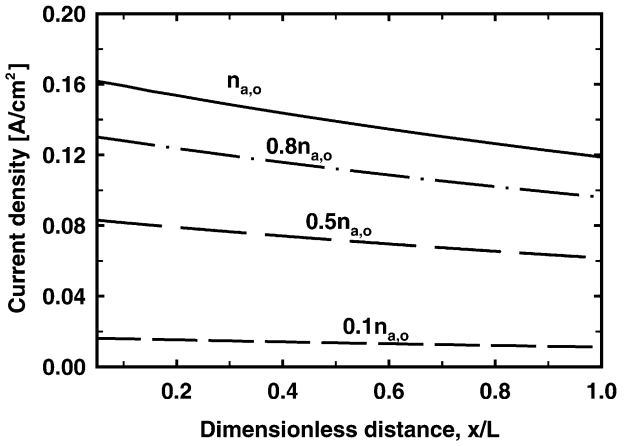

Fig. 6. Steady-state distribution of current density along direction of gas flow at different inlet anode gas-flow rates. Here, $n_{a,o}$ is the reference value of inlet anode gas-flow rate, i.e., 0.88 mol h^{-1}. Flow rates of anode and cathode gases are changed in same ratio.

than that at a small flow rate due to greater consumption of hydrogen in the electrochemical reaction.

The molar flow rates of anode and cathode gases will also affect the current density distribution in the fuel cell. Changes in the current density distribution in the fuel cell with the molar flow rate at the entrance are shown in Fig. 6. The large molar flow rate results in a high current density distribution. It also results in a large change in current density through the fuel cell.

Changes in the average current density with the molar flow rates of anode and cathode gases are presented in Fig. 7. The larger the molar flow rates, the greater are the amounts of gases that are introduced for the electrochemical reaction. Hence, the average current density is high at a larger molar flow of gases. The average current density is 0.14 A cm^{-2} at the reference conditions of this research, i.e., $n_{a,o} = 0.88$ mol h^{-1}. This value is similar to our experimental data. The power of a fuel cell is a multiplication of current and voltage. Since the cell voltage is fixed in the process of calculation, the power is proportional to the current in this research. In this respect, the time changes of the cell power at different molar flow rates are changed in the similar way as those of current density in Fig. 7.

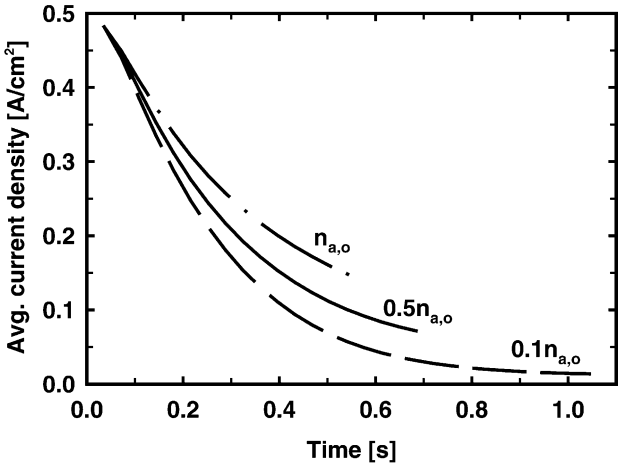

Fig. 7. Time changes of average current density at the centre of the fuel cell ($x/L = 0.5$) at $n_{a,o}$, $0.5n_{a,o}$ and $0.1n_{a,o}$. Here, $n_{a,o}$ is reference inlet anode gas-flow rate, i.e., 0.88 mol h^{-1}. Flow rates of inlet anode and cathode gases wage are changed in same ratio.

3.3. Effects of fuel utilization

The utilization of fuel gas, i.e., hydrogen, refers to the fraction of fuel gas consumed in the fuel cell. Hydrogen is consumed in the electrochemical reaction, and is also consumed or generated in the water–gas shift reaction. The fuel utilization is the sum of the results of the electrochemical reaction and the water–gas shift reaction. It depends upon the performance of the fuel cell. The effects of fuel utilization can be seen in Fig. 8, which is the graph of the total concentration of anode gas at the centre of the fuel cell ($x/L = 0.5$) versus time at different fuel utilizations. The steady-state total anode concentration is low at large fuel utilization. This can be understood in relation to Fig. 5. When the molar flow rate is large, the steady-state anode concentration is low because of the great consumption of hydrogen.

The fuel utilization also affects the time required to reach a steady-state. At a great utilization of fuel, the time is short, as shown in Fig. 8. It can be concluded that the anode gas concentration is mainly dependent upon the amount of consumed hydrogen.

Changes in the average current density with time at different fuel utilizations are given in Fig. 9. When the fuel utilization is great, more hydrogen is used in the electrochemical reaction. Hence, the current density becomes high. The average current density is 0.23 A cm^{-2} at 0.8 utilization of fuel, which is higher than 0.14 A cm^{-2} at 0.4 utilization of fuel. The graph also shows that the time to reach a steady-state is short at a high utilization of fuel, as explained in Fig. 8.

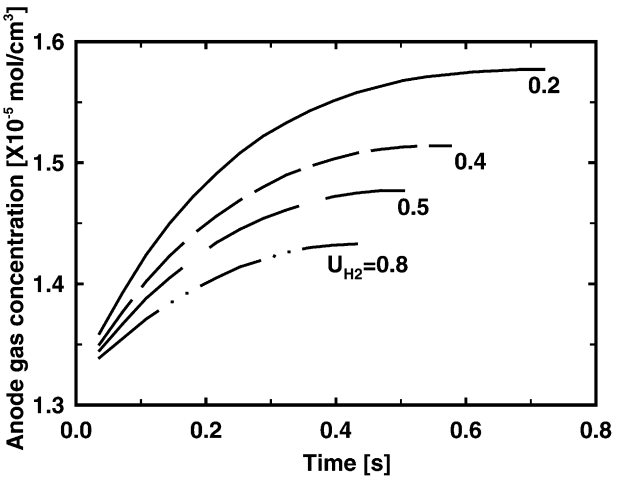

Fig. 8. Time changes of the anode gas concentration at the centre of the fuel cell ($x/L = 0.5$) for different H_2 utilization.

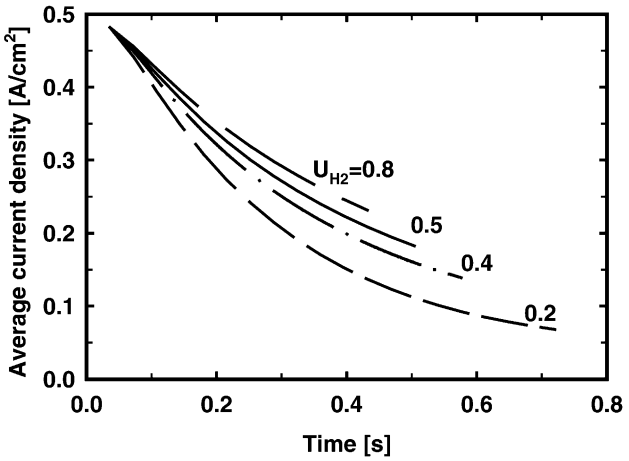

Fig. 9. Changes of average current density with time at different H_2 utilization. Here, inlet anode gas-flow rate ($n_{a,o}$) is constant at 0.88 mol h^{-1}.

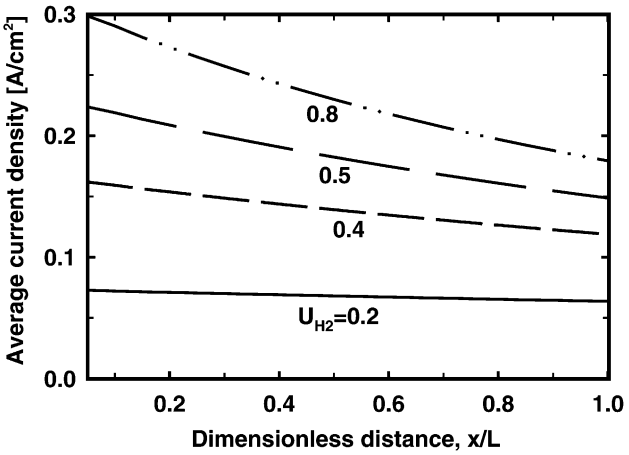

Fig. 10. Steady-state distribution of current density along direction of anode gas-flow at different H_2 gas utilization (U_{H_2}). Here, inlet anode gas-flow rate ($n_{a,o}$) is constant at 0.88 mol h^{-1}.

As time passes, the average current density decreases and reaches a steady-state. Current density distributions in the fuel cell after reaching a steady-state are presented in Fig. 10. A large utilization of fuel indicates that more hydrogen is used. Hence, the current density is high at a large utilization of fuel. At a small utilization of fuel such as $U_{H_2} = 0.2$, the change in current density through the fuel cell is very small.

4. Conclusions

Mathematical modelling of the unsteady-state of an MCFC (10 cm × 10 cm) has been studied. The behaviour of the fuel cell such as changes in electrochemical reactions, in distributions of the current density and cell temperature and in mole fractions of gases at the beginning of the operation has been examined. The effects of the molar flow rates of anode and cathode gases and the utilizations of fuel gas have been studied. The following conclusions are reached.

1. The fuel cell attains a steady-state very quickly because the size of unit fuel cell is small and the flow rate of fuel gas is large. The time to achieve a steady-state is 0.58 s and the corresponding average current density is 0.14 A cm^{-2} at the reference conditions such as 0.93 V, anode gas-flow rate 0.44 mol h^{-1} and hydrogen utilization 0.4.

   The total concentration of anode gas increases with time and reaches a steady-state value. On the other hand, that of cathode gas decreases with time and reaches a steady-state value. The average current density also decreases with time and reaches a steady-state value.
2. When the flow rate of anode gas is increased with a fixed flow rate of cathode gas, the rate of hydrogen consumption becomes faster and the distribution curve changes more rapidly along the direction of gas flow.
3. When the molar flow rates of the anode and cathode gases are high, the following results are obtained. The steady-state total concentration of anode gas is low and of the cathode is high. The current density is high and the changes in current density along the direction of gas flow are large. Time changes in cell power at different molar flow rates proceed in the same way as those of current density.
4. When the utilization of fuel, i.e., hydrogen, is high, the steady-state total anode gas concentration is low and the current density is high. Time to reach a steady-state is short.

Acknowledgements

This work was supported by the New & Renewable Energy Program in Korea. The authors acknowledge the financial support from the Korea Ministry of Trade, Industry and Energy through the R&D Management Center for Energy and Resources and the Korea Electro Power Research Institute (KEPRI).

References

[1] Y. Watanabe, M. Matsumoto, K. Takasu, J. Power Sources 61 (1996) 53.
[2] V. Sampath, A.F. Sammels, J. Electrochem. Soc. 127 (1980) 79.
[3] F. Yoshiba, N. Ono, Y. Izaki, T. Watanabe, J. Power Sources 71 (1998) 328.
[4] T.L. Wolf, G. Wilemski, J. Electrochem. Soc. 130 (1983) 48.
[5] G. Cao, M. Masubuchi, J. Jpn. Mech. Eng. Soc., B 57 (1991) 837.
[6] N. Kobayashi, H. Fujimura, K. Ohtsuka, J. Jpn. Mech. Eng. Soc., B 54 (1988) 2568.
[7] N. Kobayashi, H. Fujimura, K. Ohtsuka, J. Jpn. Mech. Eng. Soc., B 57 (1991) 825.
[8] S.W. Nam, S.H. Seo, T.H. Lim, I.H. Oh, S.A. Hong, H.C. Lim, Hydrogen Energy 3 (1992) 55.

[9] G. Lindbergh, M. Olivery, M. Sparr, J. Electrochem. Soc. 148 (2001) A411.
[10] C.G. Lee, B.S. Kang, H.K. Seo, H.C. Lim, J. Electroanal. Chem. 540 (2003) 169.
[11] B. Bosio, P. Costamagna, F. Parodi, Chem. Eng. Sci. 54 (1999) 2907.
[12] A.J. Appleby, F.R. Fouikes, Fuel Cell Hand Book, 1994, p. 539.
[13] H.K. Park, G.Y. Chung, H.C. Lim, S.W. Nam, T.H. Lim, S.A. Hong, J. Power Sources 103 (2002) 245.
[14] T.J. Kim, Y.J. Ahn, J.B. Ju, G.Y. Chung, S.W. Nam, I.H. Oh, T.H. Lim, S.A. Hong, Energy Eng. J. 4 (3) (1995) 354.
[15] Y.J. Ahn, G.Y. Chung, J.B. Ju, S.W. Nam, I.H. Oh, T.H. Lim, S.A. Hong, HWAHAK KONGHAK 32 (6) (1994) 830.
[16] H.K. Park, Y.R. Lee, M.H. Kim, G.Y. Chung, S.W. Nam, S.A. Hong, T.H. Lim, H.C. Lim, J. Power Sources 104 (2002) 140.
[17] J.M. Smith, H.C. van Ness, Introduction to Chemical Engineering Thermodynamics, fourth ed., McGraw-Hill, New York, 1987, p. 698.
[18] J.H. Koh, B.S. Kang, H.C. Lim, J. Power Sources 91 (2000) 161.
[19] J.R. Selman, Molten Salt Committee of the Electrochemical Society of Japan, 1988.
[20] Y.J. Ahn, G.Y. Chung, J.B. Ju, S.W. Nam, I.H. Oh, T.H. Lim, S.A. Hong, HWAHAK KONGHAK 33 (4) (1995) 479.
[21] M.H. Kim, G.Y. Chung, S.W. Nam, I.H. Oh, T.H. Lim, S.A. Hong, J. Energy Eng. 8 (1) (1999) 7.